

University of Groningen

Molecular Self-Doping Controls Luminescence of Pure Organic Single Crystals

Parashchuk, Olga D.; Mannanov, Artur A.; Konstantinov, Vladislav G.; Dominskiy, Dmitry I.; Surin, Nikolay M.; Borshchev, Oleg V.; Ponomarenko, Sergei A.; Pshenichnikov, Maxim S.; Paraschuk, Dmitry Yu.

Published in:
Advanced Functional Materials

DOI:
[10.1002/adfm.201800116](https://doi.org/10.1002/adfm.201800116)

IMPORTANT NOTE: You are advised to consult the publisher's version (publisher's PDF) if you wish to cite from it. Please check the document version below.

Document Version
Publisher's PDF, also known as Version of record

Publication date:
2018

[Link to publication in University of Groningen/UMCG research database](#)

Citation for published version (APA):

Parashchuk, O. D., Mannanov, A. A., Konstantinov, V. G., Dominskiy, D. I., Surin, N. M., Borshchev, O. V., Ponomarenko, S. A., Pshenichnikov, M. S., & Paraschuk, D. Y. (2018). Molecular Self-Doping Controls Luminescence of Pure Organic Single Crystals. *Advanced Functional Materials*, 28(21), [1800116]. <https://doi.org/10.1002/adfm.201800116>

Copyright

Other than for strictly personal use, it is not permitted to download or to forward/distribute the text or part of it without the consent of the author(s) and/or copyright holder(s), unless the work is under an open content license (like Creative Commons).

The publication may also be distributed here under the terms of Article 25fa of the Dutch Copyright Act, indicated by the "Taverne" license. More information can be found on the University of Groningen website: <https://www.rug.nl/library/open-access/self-archiving-pure/taverne-amendment>.

Take-down policy

If you believe that this document breaches copyright please contact us providing details, and we will remove access to the work immediately and investigate your claim.

Downloaded from the University of Groningen/UMCG research database (Pure): <http://www.rug.nl/research/portal>. For technical reasons the number of authors shown on this cover page is limited to 10 maximum.

Molecular Self-Doping Controls Luminescence of Pure Organic Single Crystals

Olga D. Parashchuk, Artur A. Mannanov, Vladislav G. Konstantinov, Dmitry I. Dominskiy, Nikolay M. Surin, Oleg V. Borshchev, Sergei A. Ponomarenko,* Maxim S. Pshenichnikov,* and Dmitry Yu. Paraschuk*

Organic optoelectronics calls for materials combining bright luminescence and efficient charge transport. The former is readily achieved in isolated molecules, while the latter requires strong molecular aggregation, which usually quenches luminescence. This hurdle is generally resolved by doping the host material with highly luminescent molecules collecting the excitation energy from the host. Here, a novel concept of molecular self-doping is introduced in which a higher luminescent dopant emerges as a minute-amount byproduct during the host material synthesis. As a one-stage process, self-doping is more advantageous than widely used external doping. The concept is proved on thiophene–phenylene cooligomers (TPCO) consisting of four (host) and six (dopant) conjugated rings. It is shown that <1% self-doping doubles the photoluminescence in the TPCO single crystals, while not affecting much their charge transport properties. The Monte-Carlo modeling of photoluminescence dynamics reveals that host–dopant energy transfer is controlled by both excitonic transport in the host and host–dopant Förster resonant energy transfer. The self-doping concept is further broadened to a variety of conjugated oligomers synthesized via Suzuki, Kumada, and Stille crosscoupling reactions. It is concluded that self-doping combined with improved excitonic transport and host–dopant energy transfer is a promising route to highly luminescent semiconducting organic single crystals for optoelectronics.

1. Introduction

Emerging organic light-emitting devices, e.g., organic light-emitting transistors (OLETs) and electrically pumped lasers, need materials combining high luminescence and efficient charge transport.^[1] The latter requires tight molecular packing, which usually results in luminescence quenching. One of the effective ways to control and enhance the light-emitting properties of organic semiconductor materials is their doping by highly luminescent molecules as commonly used in organic light-emitting diodes. For example, if the dopant absorption spectrum overlaps with the fluorescence spectrum of the host material, the host–dopant Förster resonant energy transfer (FRET) can be used to control the luminescence efficiency and spectra of the doped host material.^[2]

The most attractive materials for OLET and organic injection lasers are organic semiconducting single crystals,^[1d,3] which can also be doped by highly luminescent molecules to improve their luminescence

properties via host–dopant energy transfer.^[4] Despite the FRET effect is well understood in various donor–acceptor systems,^[5] its detailed study in organic crystals (donor) doped by luminescent molecular acceptors is still lacking. Although color tuning via donor–acceptor energy transfer was demonstrated in molecularly doped single crystals,^[6] such important issues as the optimization of the doping level and exciton diffusion, both of which can affect the host–dopant energy transfer efficiency and hence the device performance, have not been addressed.


Vapor-grown organic semiconductor single crystals with dopant-controlled and dopant-enhanced fluorescence have already been demonstrated where the host and dopant molecules were synthesized separately, their powders were milled and mixed, and finally the crystals were grown from the mixture of the two.^[4b,6] On the other hand, during the host material synthesis, small amounts of various byproducts are usually produced. If one of them is highly luminescent and has a lower optical energy gap than the host, it could serve as a dopant controlling the luminescence of the material via exciton transport in the host material and consecutive FRET to the dopant. As a result, molecular self-doping of the host by the energy acceptor is realized thereby

Dr. O. D. Parashchuk, A. A. Mannanov, V. G. Konstantinov,
D. I. Dominskiy, Prof. D. Yu. Paraschuk
Faculty of Physics and International Laser Center
Lomonosov Moscow State University
Leninskie Gory 1/62, Moscow 119991, Russian Federation
E-mail: paras@physics.msu.ru

A. A. Mannanov, Dr. M. S. Pshenichnikov
Zernike Institute for Advanced Materials
University of Groningen
Nijenborgh 4, Groningen 9747 AG, The Netherlands
E-mail: m.s.pshenichnikov@rug.nl

Dr. N. M. Surin, Dr. O. V. Borshchev, Prof. S. A. Ponomarenko
Enikolopov Institute of Synthetic Polymeric Materials
Russian Academy of Science
Profsoyuznaya 70, Moscow 117393, Russian Federation
E-mail: ponomarenko@ispm.ru

Prof. S. A. Ponomarenko
Faculty of Chemistry
Lomonosov Moscow State University
Leninskie Gory 1/3, Moscow 119991, Russian Federation

 The ORCID identification number(s) for the author(s) of this article can be found under <https://doi.org/10.1002/adfm.201800116>.

DOI: 10.1002/adfm.201800116

removing the necessity to synthesize the dopant separately. Moreover, in this manner, one avoids complicated purification of the host organic semiconductor from the dopant; accordingly, the overall cost of the material could be substantially reduced. This approach radically differs from both physical self-doping used earlier to dope the amorphous phase of polyfluorene by its β -phase,^[7] and self-doping by charges recently demonstrated within one molecule (perylene diimide) by amine substituents.^[8]

In this work, we introduce the concept of molecular self-doping as a novel approach to control the luminescence of nominally chemically pure (>99%) conjugated organic materials. For this purpose, we used thiophene–phenylene co-oligomer (TPCO) single crystals, which combine pronounced luminescence and efficient charge transport.^[9] As the host material, we synthesized TPCO with the molecular structure 5,5'-bis[4-(trimethylsilyl)phenyl]-2,2'-bithiophene (TMS–P2TP–TMS),^[9a] where P and T stand for 1,4-phenylene and 2,5-thiophene, respectively; TMS is trimethylsilyl group. We found that a longer TPCO, 5,5'''-bis[4-(trimethylsilyl)phenyl]-2,2':5',2'':5'',2'''-quaterthiophene (TMS–P4TP–TMS) that emerges in minute amounts (<1%) as a byproduct during the host synthesis acts as an efficient energy acceptor of the host excitation energy in the crystal. To identify and quantify such a minute amount of dopant that is chemically very similar to the host, we applied a photoluminescent (PL) method with sensitivity to dopant down to 100 ppm level at the presence of the host of a very similar molecular structure. The optimal doping doubles the PL quantum yield (QY) of the solution-grown TPCO single crystals while retaining the efficient charge transport properties. Monte-Carlo (MC) modeling of the PL time-resolved spectra recorded in variously doped crystals was used to reveal the interplay between exciton diffusion in the host material and FRET to the dopant. We further broadened the scope of the self-doping concept onto other molecular crystals, which were grown from various conjugated oligomers synthesized via different chemical routes. Our findings clearly demonstrate that molecular self-doping combined with enhanced excitonic transport and host–dopant energy transfer paves the way to highly luminescent semiconducting organic crystals for optoelectronics applications.

2. Results

2.1. Material Synthesis and Crystals Growth

To synthesize self-doped TMS–P2TP–TMS material, we used the synthetic route (Figure 1a) based on Pd-catalyzed Suzuki crosscoupling between trimethyl[4-(4,4,5,5-tetramethyl-1,3,2-dioxaborolan-2-yl)phenyl]silane (1) and 5,5'-dibromo-2,2'-bithiophene (2). At the first stage, a monosubstituted intermediate product, 5-bromo-5'-[4-(trimethylsilyl)phenyl]-2,2'-bithiophene (3), is formed, further reaction of which with compound 1 leads to the final product TMS–P2TP–TMS. However, exchange of the boronic acid residue of compound 1 with the bromine of compound 2 or 3 within the catalytic cycle eventually gives rise to a byproduct 5-[4-(trimethylsilyl)phenyl]-5'-(4,4,5,5-tetramethyl-1,3,2-dioxaborolan-2-yl)-2,2'-bithiophene (4), reaction of which with compound 3 results in a longer TPCO, 5,5'''-bis[4-(trimethylsilyl)phenyl]-2,2':5',2'':5'',2'''-quaterthiophene (TMS–P4TP–TMS). A step-by-step scheme of its formation is described in Section 1 in the Supporting Information. As a result, this route leads to the host material TMS–P2TP–TMS doped by longer TPCO TMS–P4TP–TMS (dopant) as a byproduct, i.e., TMS–P2TP–TMS is self-doped by TMS–P4TP–TMS. The self-doping level in the crude powder after the standard purification by column chromatography on silica gel (eluent—hot toluene) followed by recrystallization from toluene (see Experimental Section) was found to be 1.4%; using subsequent vacuum sublimations, we obtained the molecular self-doped host powders doped in the range of 0.01–0.05%. Samples with the doping range of 0.1–1.4% were prepared by mixing the lowest (0.01%) and the highest (1.4%) self-doped materials with precalculated ratios; we will also refer to such samples as self-doped. TMS–P4TP–TMS (dopant) was also synthesized separately (see Figure 1b) to dope the host externally, the pristine dopant was also needed for its quantitative identification in the doped host material. Thus, the synthesis of the host was the same for self and external doping, and the difference was only in the purification of the raw host material.

Differential scanning calorimetry (DSC) data for the self-doped crude samples indicate the only crystalline phase

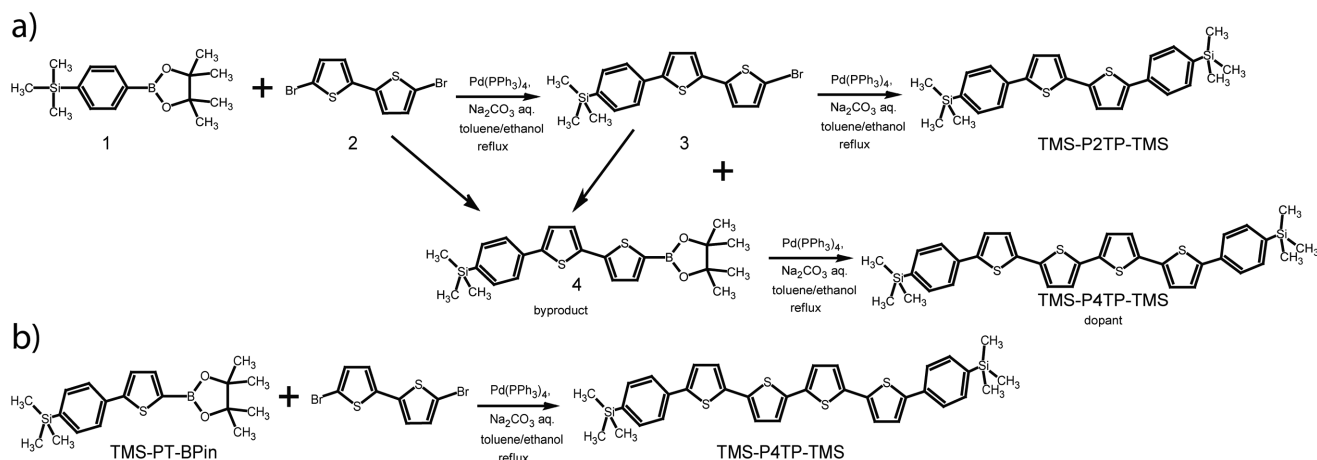


Figure 1. Implementation of the self-doping concept. a) Synthetic route of TMS–P2TP–TMS (host) doped by TMS–P4TP–TMS (dopant) as a byproduct. b) Scheme of synthesis of TMS–P4TP–TMS.

(Section 2, Supporting Information). Crystals grown from solution of the doped host powders (for the micrographs, see Figure S4a, Supporting Information) had the same doping levels as the parent powders used for crystal growth (Figure S5, Supporting Information). At the low doping levels, the single crystals had a shape of smooth flat square plates with a lateral size of about 1–5 mm and a thickness from a half to a few μm (Figure S4a, Supporting Information). In contrast, the heavily ($\approx 1\%$ and higher) doped crystals contained many visible defects, which suggests that the dopant impedes the crystal growth by inducing growth defects. The crystals prepared by external and self-doping did not differ visually from each other (Figure S4a, Supporting Information).

2.2. Photoluminescence

Figure 2 summarizes absorption, PL spectra of the host (TMS–P2TP–TMS), dopant (TMS–P4TP–TMS) in solution (a), and doped host crystals (b,c). To prove host–dopant energy transfer, the PL spectrum of the pure host crystal (i.e., whose luminescent properties are not affected by the dopant) is needed as a reference. However, from our numerous unsuccessful attempts to purify the host material from the dopant above 99.99% (by using multiple vacuum sublimations, vapor crystal growth, solution recrystallization), we concluded that the dopant molecules are firmly embedded in the host crystal and do not form their own phase, which could be detected by X-ray diffraction or DSC (Section 2, Supporting Information). As a result, PL from the lowest doped (0.01%) crystal was used as the reference. Figure 2b compares this reference PL with the PL excitation spectra of the lowest and highly doped host crystals, the grey area illustrates a noticeable overlap between the host PL and the dopant optical absorption thereby promising efficient energy transfer of the host excitation via, e.g., FRET to the dopant. The dopant PL QY in solution was measured as $44 \pm 2\%$, which is a factor of two higher than that of the host ($20 \pm 2\%$). This makes it feasible to tune the luminescence spectrum and enhance QY in the doped host crystal utilizing host–dopant energy transfer via exciton diffusion in the host matrix with consecutive host–dopant FRET.

The host (dopant) PL and absorption spectra noticeably overlap (see the blue and black lines for the host, and the red and magenta lines for the dopant in Figure 2a). As a result, PL spectra in the crystals are expected to be affected by PL reabsorption, which is further enhanced by strong waveguiding observed in various TPCO single crystals.^[1d] To minimize the effect of both, we mechanically grinded the doped crystals into powder.^[10] Figure 2c compares PL spectra of the grinded (solid lines) and as-grown (dashed lines) TMS–P2TP–TMS crystals with the lowest (0.01%) and highest (3%) doping levels. It clearly shows that the PL red shift is caused by both doping and PL reabsorption. The doping-induced red shift could be assigned to host–dopant energy transfer (see below). Remarkably, the PL spectra of the grinded lowest and highest doped crystals (Figure 2c) virtually reproduce those of dopant and host solutions (Figure 2a), respectively; an ≈ 0.1 eV shift caused by the solid-state phase notwithstanding. Accordingly, the dopant in the lowest doped crystal does not affect

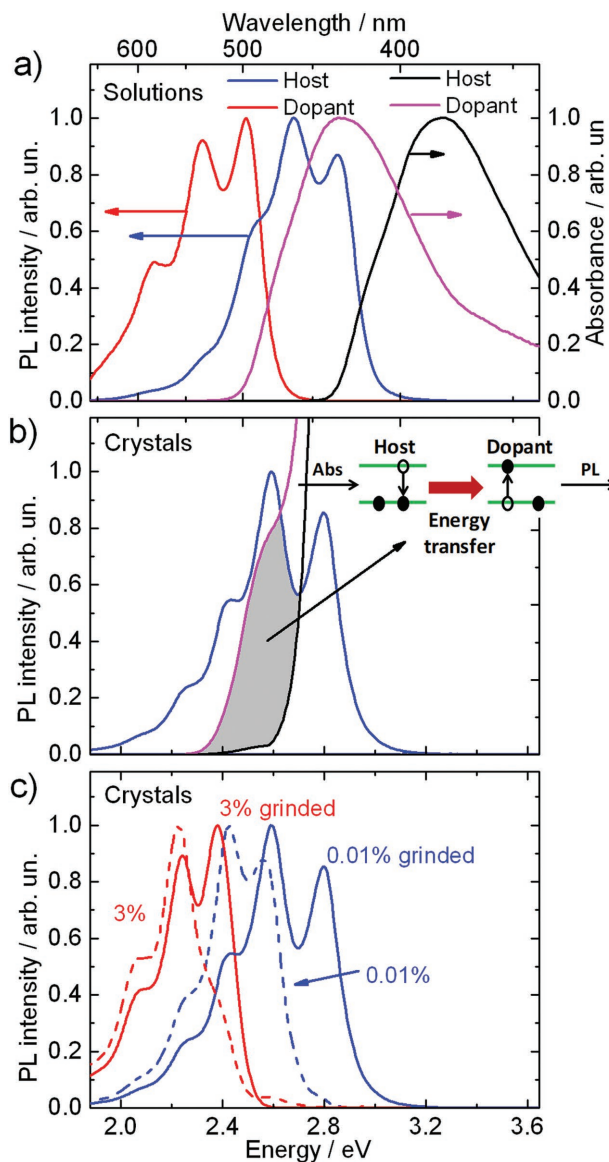


Figure 2. Steady-state PL and absorption spectra. a) Absorption and PL spectra of the host (TMS–P2TP–TMS) and the dopant (TMS–P4TP–TMS) in THF solutions. The PL excitation wavelength was set at 300 nm for the host and 375 nm for the dopant; b) Illustration of the feasibility of FRET in TMS–P2TP–TMS crystals doped by TMS–P4TP–TMS. As the PL spectrum of the donor (host), PL of the grinded lowest doped (0.01%) crystal is shown by the blue line; grinding was used to decrease the PL reabsorption. The magenta and black lines demonstrate the PL excitation spectra of the lowest and highly doped TMS–P2TP–TMS crystals (for details see Figure S6d, Supporting Information), the shoulder at ≈ 2.55 eV is assigned to the dopant absorption. The inset illustrates FRET in the doped host. The grey area in panel (b) indicates the spectral overlap between host PL and dopant absorption required for FRET; c) PL spectra of as-grown (dash lines) and grinded (solid lines) doped TMS–P2TP–TMS crystals, the doping levels are shown in the plot. The solid blue line (PL of the grinded 0.01% doped crystal) is duplicated from panel (b) for comparison. The PL excitation wavelength was set at 405 nm.

the crystal PL, whereas nearly all PL comes from the dopant in the highest doped crystal, which implies complete host–dopant energy transfer. Thus, we conclude that the PL spectra

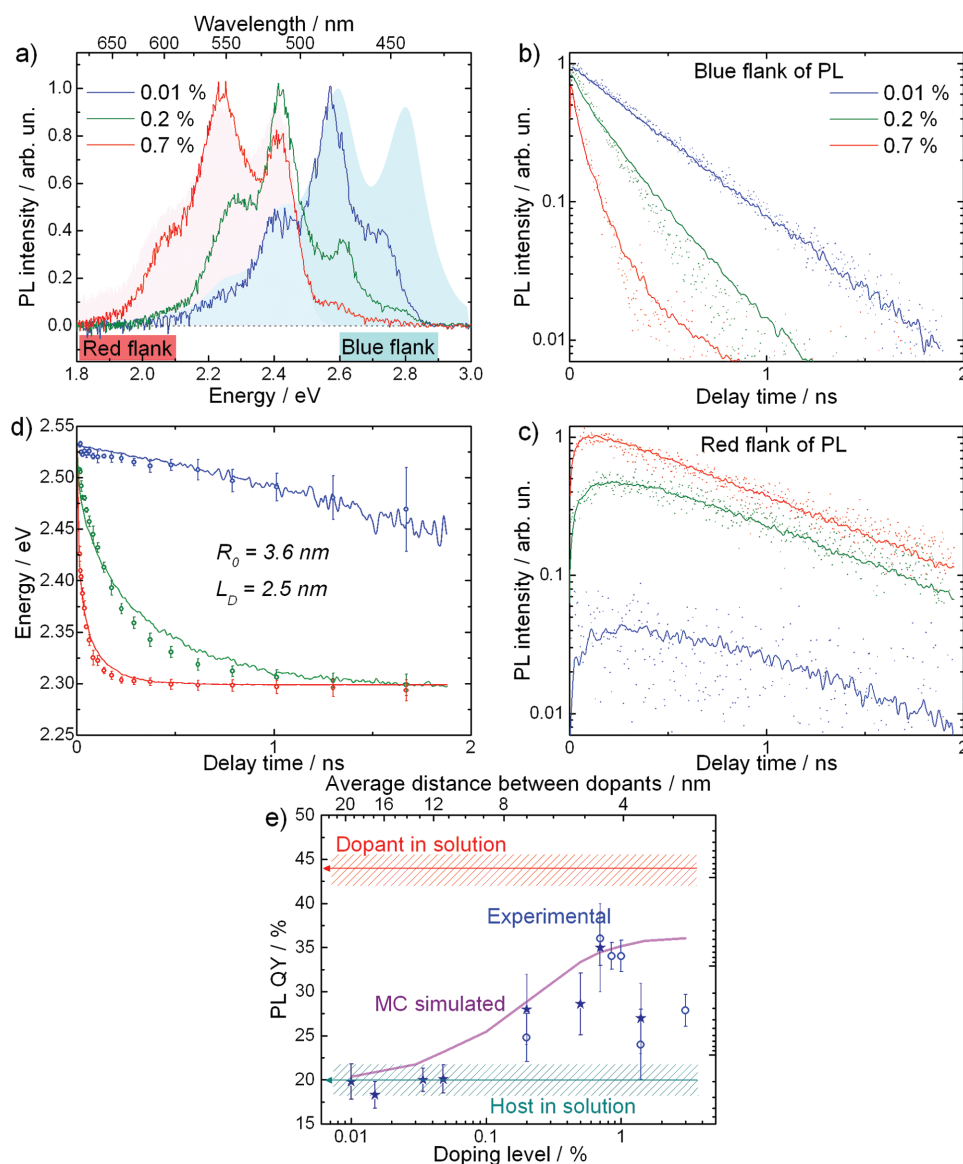


Figure 3. PL data of the doped crystals. a) PL spectra in a few self-doped crystals after 400 nm excitation (lines), obtained from the streak-camera PL maps integrated over the 0–2 ns time window, in the microscopic configuration (for the PL maps, see Figure S9, Supporting Information). The cyan- and red-shaded spectra represent, respectively, the reference spectra of the grinded 0.01% doped crystal from Figure 2b (the host PL spectrum) at 405 nm excitation and the 0.7% doped crystal at 465 nm excitation, where mostly the dopant is excited. b,c) PL transients extracted from the PL maps at the blue and red PL spectral flanks (indicated in (a) by the blue and red rectangles) originated mostly from host and dopant PL, respectively. Dots are the experimental data; the lines are the outcome of the MC simulations. Scaling between the experimentally obtained and simulated PL intensities is preserved. For the 0.7% doped crystal, dopant PL begins to dominate at long times, which leads to the biexponential decay of the transient. d) Experimental (circles) and MC simulated (solid lines) dynamical red shifts of the mean PL energy. Solid lines depict the MC simulated mean energy values with the following output parameters: the Förster radius of $R_0 = 3.6$ nm and the exciton diffusion length of $L_D = 2.5$ nm (see Section 14, Supporting Information). e) Experimental (symbols) and MC simulated (the purple line) PL QY values as functions of the doping level. The blue open dots and navy stars show the data for externally and self-doped crystals, respectively. The horizontal lines demonstrate the host and dopant PL QYs in solution, the experimental accuracy is depicted by hatching. The upper axis in (e) shows an average distance between the dopants in the host crystals (Section 8, Supporting Information).

of the grinded crystals are almost free of PL reabsorption so that grinding was used for evaluation of PL QY in the crystals (see below). To focus on the host–dopant energy transfer process, one needs to minimize the PL reabsorption effect on the PL spectra of variously doped crystals. For this, their PL was collected in the microscopic configuration so that the PL

pathway in the crystals was about their thickness (≈ 1 μ m) or less.

Figure 3a shows PL spectra of the self-doped crystals at three representative doping levels together with the reference host and dopant spectra (marked as the shaded areas). Upon increase of the doping level, the PL spectra shift to the red from

one reference spectrum to another, which is attributed to the increased share of the red-shifted dopant PL (for the complete set of PL spectra in the doped crystals, see Figure S6a, Supporting Information). As direct dopant excitation at 400 nm is negligible due to low dopant concentration, the observed PL features are assigned to host–dopant energy transfer. Host and dopant PL exhibit identical polarization properties (Figure S7, Supporting Information), which suggests that the dopant molecules substitute the host sites in the doped crystals as was earlier reported for other doped TPCO crystals.^[4b] Although the dopant molecule has a similar shape but a longer length as compared with the host ones, it could substitute the host one with minor deformations of dopant and a few adjacent host molecules, which is confirmed by molecular dynamics simulation (Section 7, Supporting Information).

To prove the energy transfer between the host and dopants, we recorded PL transients at the blue and red flanks of PL spectra (Figure 3a), which correspond mainly to host and dopant PL, respectively (Figure 3b,c). Decay of the host PL (Figure 3b) accelerates from ≈ 0.4 to 0.1 ns with increasing the doping level. Correspondingly, dopant PL (Figure 3c) acquires a raising component with the time that is similar to the blue-flank decay (0.07–0.2 ns; Figure S11c, Supporting Information). Shortening of decay times of the blue-flank transients with doping and the corresponding rise in the red-flank transients are fully consistent with host–dopant energy transfer. Finally, PL at the red flank decays considerable longer as compared with the blue flank (0.7–0.8 vs 0.07–0.4 ns) again confirming its origin from the dopant.

Another convenient way to characterize the energy transport process in the crystals is to analyze the dynamical red shift of the mean PL energy (Figure 3d and Section 10c, Supporting Information). For the lowest doping level, PL originates mostly from the host excitons (mean energy of ≈ 2.55 eV), with a weak PL shift to the red due to energy transfer to the dopants. At the doping level of 0.2% and higher, the majority of excitons in the crystal are transferred to the lower energy levels with the red-shifted PL energy of ≈ 2.3 eV, which corresponds to the dopant PL. The low-temperature transient PL data demonstrate that the host–dopant energy transfer is weakly temperature-dependent (see Section 11, Supporting Information), which is consistent with FRET domination over exciton diffusion.

Efficient host–dopant energy transfer enhances PL of the doped host crystals. However, strong PL reabsorption results in underestimation of the PL QY values in the as-grown crystals (Figure S17c, Supporting Information). To correct the PL QY measured in the as-grown crystals for PL reabsorption, we applied two methods (for more details, see Section 12, Supporting Information). Parker's one^[11] is based on deconvolution of the experimental PL spectrum into a linear combination of the reabsorption-free PL spectra of the host crystal and the dopant in host crystal (cyan- and red-shaded spectra in Figure 3a, respectively). The second PL reabsorption correction method is based on comparison of the PL spectra of the as-grown and grinded crystals.^[9b,12] Both methods provide very close values of the reabsorption-corrected PL QY (Figure S17c, Supporting Information).

Reabsorption-corrected PL QYs calculated by Parker's method are shown in Figure 3e as a function of the doping

level. In the 0.7% doped (referred further on as an optimally doped) crystal, PL QY climaxes at almost 40%, which is close to that of the dopant in solution (the red line in Figure 3d). In the lowest doped crystal (0.01%), PL QY of $\approx 20\%$ is equal to that of the host molecule in solution (the aqua line in Figure 3d). This fully corroborates the time-resolved data where the optimally doped crystals show the fastest host PL decay time (Figure S13a, Supporting Information). In the crystals doped at $>1\%$, PL QY decreases, and the host–dopant energy transfer becomes less efficient (Figures S13a and S15b, Supporting Information). This is explained by aggregation of dopant molecules, which also results in the visible defects in the highly doped samples (Figure S4a, Supporting Information). Note that the PL QY data (Figure S17c, Supporting Information) as well as PL spectral data (Figures S6c and S9, Supporting Information) are virtually identical for the self- and externally doped samples; therefore, the two doping techniques result in the optically indistinguishable crystals.

2.3. MC Simulations

To support the FRET mechanism of host–dopant energy transfer and unravel the balance between exciton diffusion and FRET in host–dopant energy transfer, we performed MC simulations of the energy transport in the host matrix with randomly distributed dopants (see Section 13, Supporting Information). The simulated data describe well the experimental PL transients and red shifts (Figure 3b–d) and the experimental PL QY (Figure 3e) at the doping levels up to the optimal one. At the higher doping levels, the obvious discrepancy between the simulated and experimental PL QYs is explained by the fact that the dopant aggregation was not included in the MC simulations.

From the MC simulation (see Sections 14–16, Supporting Information), the Förster radius R_0 was obtained as 3.6 ± 0.2 nm, which corroborates the value of 4.0 nm calculated directly from the Förster equation (for details, see Section 17, Supporting Information). The exciton diffusion length amounts to $L_d = 2.5 \pm 0.4$ nm, which is at the short side of the known exciton diffusion lengths of ≈ 5 –10 nm in amorphous organic films.^[13] This is ascribed to weak intermolecular interaction in the host crystal as the coupling between the transition dipole moments of the nearest molecules corresponds to weak J-aggregation (see Figure S3, Supporting Information in ref. [9b]). Weak J-aggregate-type coupling also explains why the host crystal PL QY equals to that of diluted host molecules. In the optimally doped crystal, about 90% of the initial host excitons transfer their energy to the dopants (Figure S21, Supporting Information) mostly via FRET, i.e., the majority of the host excitons are already generated within the Förster radius from the dopant (for the interplay between FRET and exciton diffusion, see Section 15, Supporting Information).

2.4. Charge Transport

We have established that molecular self-doping enhances PL of organic crystals; but does it affect their charge transport

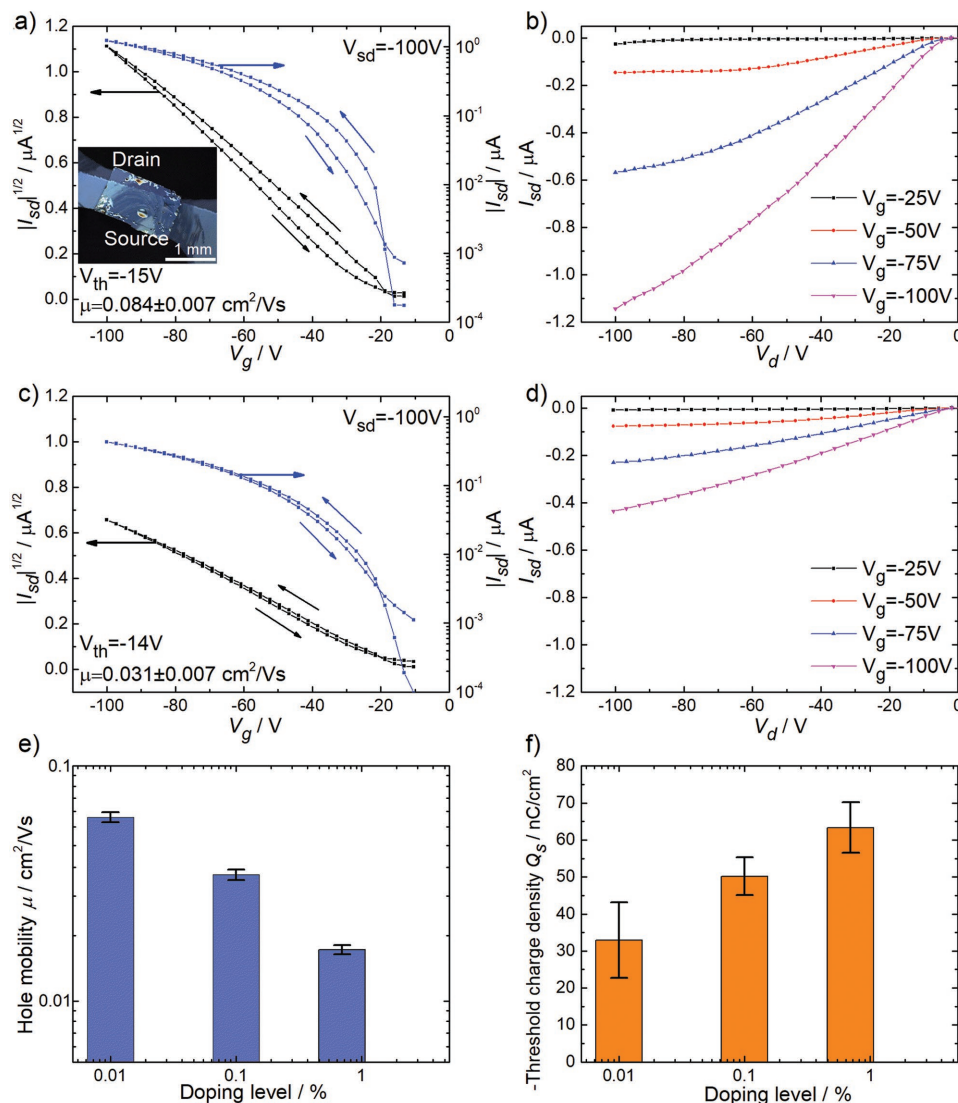


Figure 4. OFET data for self-doped crystals. Transfer (a,c) and output (b,d) characteristics of best single-crystal OFETs for self-doping level 0.01% (a,b) and 0.7% (c,d). Optical image of a crystal with the source and drain graphite contacts is shown in the inset. Hole mobility (e) and threshold charge density (f) calculated from the threshold voltage, each data point is an average over 6–8 devices (Table S2, Supporting Information).

properties? **Figure 4** summarizes charge transport data recorded in organic field-effect transistors (OFETs) based on the self-doped TMS–P2TP–TMS single crystals, the full OFET data are presented in Table S2 and Figure S25 in the Supporting Information. As panels a–d show, OFETs on the self-doped crystals demonstrate clear *p*-type behavior with small hysteresis. The charge mobility is among the best reported for other TPCO single crystals.^[14] Increasing the doping level somewhat degrades the charge transport resulting in lower charge mobility and higher threshold charge density as shown in Figure 4e,f. With the doping level increased by a factor of almost 100, the hole mobility in the optimally doped crystal decreases by a factor of ≈ 4 as compared with the lowest doped one ($0.06 \text{ cm}^2 \text{ V}^{-1} \text{ s}^{-1}$), while the threshold charge density doubles. We explain this as follows: the dopant affects charge transport in the host inducing deep or/and shallow traps for moving charges as the dopant highest occupied (lowest unoccupied) orbital energy is higher

(lower) than the host one (see Section 20, Supporting Information). In organic field-effect devices, the deep traps determine the threshold voltage (charge density), and the shallow traps control the charge mobility according to the multiple trap and release model.^[14] All in all, the detrimental impact of the dopants charge transport in the host crystals is rather moderate, and therefore self-doped single crystals could be used in OLETs and current-driven organic lasers.

3. Discussion

We have harnessed the byproduct of Suzuki reactions to synthesize a doped organic semiconductor with enhanced luminescence as proved by steady-state and time-resolved optical spectroscopy. However, formation of byproducts due to ligand exchange within the organometallic catalytic cycle is known

not only for Suzuki but also for other Pd-catalyzed crosscoupling reactions used for synthesis of conjugated materials.^[15] To demonstrate that the molecular self-doping is not limited to a single aforementioned case, we studied different conjugated oligoarylenes synthesized via Suzuki, Kumada, and Stille crosscoupling reactions: TPCOs, oligophenylene, and furan/phenylene cooligomer with various conjugated lengths and terminal substituents (Section 21, Supporting Information). All these reactions produce self-dopants with longer conjugation lengths as minor byproducts. The time-resolved PL data on crystals of these oligomers clearly indicate prominent energy transfer from the host to the self-dopants (Section 21c, Supporting Information), which broadens the scope of the self-doping approach.

As the accuracy of standard techniques used to prove the purity of organic materials (NMR, high-performance liquid chromatography, gel permeation chromatography (GPC) elemental analysis, and mass spectroscopy) might miss such minor byproducts, we believe that the effect of these tiny-amount molecular self-dopants on the luminescent properties of the nominally chemically pure materials has been largely overlooked in the past. In our view, the self-dopant molecules are embedded in host crystal matrix substituting the host sites as was demonstrated above for TMS–P2TP–TMS/TMS–P4TP–TMS, i.e., the host and dopant form cocrystals.^[16] Despite much less solubility of the self-dopants in organic solvents as compared with the host, the self-dopant does not precipitate during self-doping, but it is incorporated in the host crystal. This can be explained by complex formation between the dopant and host molecules already in solution as both have the similar rod-like molecular structures so that they stick together with their molecular axes having nearly the same orientation. These complexes survive in the course of further processing including cocrystallization so that the dopant substitutes the host sites in the host crystal lattice. As a result, complete purification of the host from the dopant is a complicated task.

It might well be possible that unintentional doping by longer oligomers also occurred in numerous earlier luminescent studies in nominally chemically pure (>99%) solid samples of conjugated oligomers synthesized via metal-catalyzed crosscoupling reactions. As shown herein, the luminescent dopant even at low content (<1%) in the host material could strongly affect its luminescent properties. This may be one of the reasons for poor understanding of the luminescent properties of conjugated materials, as a very minute amount of dopants can be sufficient to drastically change the luminescence in host–guest systems based on conjugated oligomers.^[17] For example, if the self-dopant is low-emissive, it may quench luminescence of the material via host–dopant energy transfer, limiting the exciton diffusion length and resulting in nonradiative losses of excitation energy. Accordingly, molecular self-doping can be detrimental in materials for organic photovoltaics, where long exciton diffusion length is a prerequisite for high performance of organic solar cells.^[18] On the other hand, by finding an appropriate route for the host material synthesis, molecular self-doping could be applied to a vast variety of conjugated oligomers as a means to control their luminescence by a minute amount of dopant. Agreeably, the control of the self-doping level is an important issue for applications. In the

TMS–PTTP–TMS/TMS–P4TP–TMS host–dopant system, the synthesized crude powder had a reproducible doping level of about 1%, which accidentally was very close to the optimal doping level needed for applications. Nonetheless, in the TMS–PTTP–TMS/TMS–P4TP–TMS system, the self-doping level is readily controlled via vacuum sublimations; in other materials (see Section 21, Supporting Information), the self-doping level can also be controlled during solution processing, which is more promising for practical applications. Basically, solution processing in the course of chemical synthesis grants a plenty of opportunities to control the self-doping level as the host and the self-dopant have similar but different molecular structures and, therefore, much or less different physical and chemical properties. For example, using the strong difference in solubility of the self-dopant and host molecules, one could control the self-doping level during the chemical synthesis by using appropriate solvents and temperature.

4. Conclusion

To summarize, we have introduced the molecular self-doping concept as a novel approach to controlling the luminescence in single crystals prepared from nominally chemically pure conjugated oligomers via excitonic transport and host–dopant energy transfer. We have demonstrated that molecular self-doping operates in various conjugated oligomers synthesized via different Pd-catalyzed crosscoupling reactions so that their luminescence in solid-state is strongly affected by the self-dopants. Self-doping offers a number of attractive benefits as compared to more conventional external molecular doping. First, the byproducts produced during the host synthesis could be shorter or longer than the host oligomers. The former are easily removed by standard purification, while the latter remain due to their lower solubility, ensuring the red-shifted dopant absorption spectrum, which is necessary for efficient host–dopant FRET. Second, molecular self-doping provides suitable dopant oligomers in tiny amount immediately in the host powder; therefore, there is no need to synthesize and process the dopant separately which lowers the costs of the chemical synthesis and purification. Finally, the longer dopant is typically less soluble that rises the solubility issues for external doping but not so critical for self-doping, where the host molecules probably impede dopant aggregation. The moderate but still detrimental effect of doping on the charge transport can be reduced by exciton transport optimization, which would lead to even lower doping levels to facilitate highly efficient host–dopant energy transfer. In a broader context, the molecular self-doping concept is deemed as a promising route for designing the perspective organic optoelectronic materials compatible with solution-based technologies of organic electronics.

5. Experimental Section

TPCO Synthesis: 5,5'-bis(4-(trimethylsilyl)phenyl)-2,2'-bithiophene (TMS–P2TP–TMS) was synthesized according to the procedure reported elsewhere.^[9a] Pristine TMS–P4TP–TMS was synthesized via coupling of trimethyl[4-[5-(4,4,5,5-tetramethyl-1,3,2-dioxaborolan-2-yl)thiophen-2-yl]phenyl]silane (TMS–PT–BPIn)^[19] with 5,5'-dibromo-2,2'-bithiophene

under Suzuki conditions (Figure 1b). The GPC data, results of NMR analysis, sublimation technique, reagents, solvents, and TMS–P4TP–TMS detailed synthesis are presented below.

Characterization: GPC analysis was performed by means of a Shimadzu LC10AVP series chromatograph equipped with an RID-10AVP refractometer and SPD-M10AVP diode matrix as detectors and a Phenomenex column with a size of $7.8 \times 300 \text{ mm}^2$ filled with the Phenogel sorbent with a pour size of 500 Å; tetrahydrofuran (THF) was used as the eluent. Glassware was dried in a drybox at 150 °C for 2 h, assembled while hot, and cooled in an argon stream. For thin layer chromatography, “Sorbfil” plates were used. In the case of column chromatography, silica gel 60 (Merck) was used.

¹H NMR spectra were recorded at a Bruker WP-250 SY spectrometer, working at a frequency of 250.13 MHz and utilizing CDCl₃ signal (7.25 ppm) as the internal standard. In the case of ¹H NMR spectroscopy, the compounds to be analyzed were taken in the form of 1% solutions in CDCl₃. The spectra were then processed using the ACD Labs software.

Sublimation Method: The TMS–P4TP–TMS concentration in the TMS–P2TP–TMS powder was varied by a number of subsequent vacuum sublimations by Aldrich sublimation apparatus at vacuum level 0.2–0.3 mbar upon heating in an oil bath to 210 °C.

Reagents and Solvents: Tetrakis(triphenylphosphine) palladium(0) Pd(PPh₃)₄ was obtained from Sigma-Aldrich Co. and used without further purification. 5,5′-dibromo-2,2′-bithiophene and trimethyl[4-[5-(4,4,4,5,5-tetramethyl-1,3,2-dioxaborolan-2-yl)thiophen-2-yl]phenyl]silane (TMS–PT–BPIn)^[19,20] were synthesized according to procedures published elsewhere. Toluene and ethanol were dried and purified according to the standard techniques and then used as solvents.

5,5′′-bis(4-trimethylsilylphenyl-1-yl)-2,2′:5′,2′′:5′′,2′′′-quaterthiophene (TMS–P4TP–TMS): In inert atmosphere, degassed solutions of trimethyl[4-[5-(4,4,4,5,5-tetramethyl-1,3,2-dioxaborolan-2-yl)thiophen-2-yl]phenyl]silane (TMS–PT–BPIn) (1.35 g, 3.8 mmol) and 5,5′-dibromo-2,2′-bithiophene (0.51 g, 1.6 mmol) in toluene–ethanol mixture (40/4 mL) and 2 M solution of aq. Na₂CO₃ (40 mL) were added to Pd(PPh₃)₄ (50 mg, 0.04 mmol). The reaction mixture was stirred under reflux for 24 h, and then it was cooled to room temperature and poured into 150 mL of water and 250 mL of toluene. The organic phase was separated, washed with water, dried over sodium sulfate, and filtered. The solvent was evaporated in vacuum, and the residue was dried at 1 Torr. The crude product was purified by passing through silica gel column (eluent: hot toluene) followed recrystallization from toluene to give pure compound TMS–P4TP–TMS (0.7 g, 71%) as orange solid. *mp* = 307 °C. ¹H NMR (250 MHz, CDCl₃, δ): 0.30 (s, 18H, Si–CH₃), 7.50–7.20 (overlapped signals, 8H), 7.50–7.62 (overlapped signals, 8H). ²⁹Si NMR (60 MHz, DMCO-d₆): δ -4.07.

Doping and Crystal Growth: The crude TMS–P2TP–TMS (host) powder self-doped by TMS–P4TP–TMS (dopant) was subsequently sublimed in vacuum to prepare self-doped host powders with different doping levels. A number of doped host powders were prepared by external doping, i.e., by mixing the lowest self-doped host and pristine dopant powders at prescribed host–dopant molar ratios to compare with the self-doped samples and to extend the doping range to higher doping levels.

Doped host powders were dissolved in toluene with a concentration of 1.3 g L⁻¹. Doped host crystals were grown by the solvent–antisolvent crystallization method.^[9a] Host and dopant crystals were also grown from vapor by physical vapor transport (Section 3, Supporting Information). The X-ray diffraction, crystal structure, and atomic-force microscopy data for TMS–P2TP–TMS crystals were reported earlier.^[9a] Differently doped crystals showed indistinguishable X-ray diffraction patterns, which suggest that the dopant molecules were embedded in the host crystal and did not form their own phase. After the growth, the few-micrometer thick crystals were transferred on glass substrates. The TMS–P4TP–TMS content in the doped powders and crystals was determined by optical absorption and PL spectroscopy as described in Section 5 in the Supporting Information.

Photoluminescence: PL spectra and QY in solutions were measured as described in Section 6 in the Supporting Information. The steady-state

PL spectra and QY of the solid samples (unless otherwise specified) were measured using an integrating sphere (Newport 819C-SL-3.3) optically coupled to a Raman microscope (InVia, Renishaw) at an excitation wavelength of 405 nm as described in ref. [12b]. Time-resolved PL under 100 fs, 400 nm excitation was measured by a streak camera (C5680, Hamamatsu) combined with a polychromator (for the details of polarization-resolved, room and low temperature measurements, see Sections 7, 9, and 11 in the Supporting Information, respectively).

MC Simulations: MC simulations were performed as a random walk of excitons in a 3D cubic crystal grid with a subsequent FRET to the dopants (Section 13, Supporting Information.).

OFET: OFET samples based on the self-doped single crystals were fabricated using the top-contact top-gate configuration used earlier in refs. [9b,12b,21] (Section 18, Supporting Information). The saturation mode was used for calculation of the charge mobility in the OFET samples (see Equation S8, Supporting Information).

Supporting Information

Supporting Information is available from the Wiley Online Library or from the author.

Acknowledgements

O.D.P. and A.A.M. contributed equally to this work. The authors thank V. V. Bruevich for grateful assistance in photoluminescence quantum yield measurements, L. G. Kudryashova and O. V. Kozlov for their PL transient data at the early stage of the project, F. de Haan for the MC simulations code, A. Yu. Sosorev for DFT calculations, and J. Gierschner for fruitful discussions and especially his remark on the potentially high impact of minute impurities in organic semiconductors on their luminescence. The authors gratefully acknowledge contributions by M. S. Kazantzev for the furan-phenylene cooligomer (BPFB) samples, Yu. N. Luponosov for the Hex-TTPPT-Hex samples, V. A. Trukhanov and V. A. Postnikov for vapor and solution growth of the TMS–4P–TMS crystals, respectively. Also, the authors thank V. A. Tafenko for X-ray diffraction studies. The work on chemical synthesis was financially supported by the Russian Science Foundation (#15-12-30031). The work on material purification was performed in the framework of Leading science school #NSH-5698.2018.3 supported by the Ministry of Education and Science of the Russian Federation. The work on steady-state PL and electrical measurements was financially supported by the Russian Foundation for Basic Research (#17-02-00841). O.D.P. thanks the Oleg Deripaska Foundation «Volnoe Delo» (#D1-17/013-03) for support of the work on crystal growth and external doping. D.Y.P. acknowledges financial support of his work in Groningen from the Aurora program (Erasmus Mundus Action 2). Time-resolved PL experiments and MC modeling were funded by the Dieptestrategie Programme of the Zernike Institute for Advanced Materials (University of Groningen, the Netherlands). Crystal growth and measurements of steady-state PL were performed at the equipment purchased under the Lomonosov Moscow State University Program of Development.

Conflict of Interest

The authors declare no conflict of interest.

Keywords

charge transport, Förster resonant energy transfer, organic electronics, Suzuki reaction, thiophene–phenylene cooligomers

Received: January 5, 2018
Revised: February 5, 2018
Published online: March 12, 2018

- [1] a) G. E. Jabbour, S. E. Shaheen, M. M. Morrell, J. D. Anderson, P. Lee, S. Thayumanavan, S. Barlow, E. Bellmann, R. H. Grubbs, B. Kippelen, S. Marder, N. R. Armstrong, N. Peyghambarian, *IEEE J. Quantum Electron.* **2000**, *36*, 12; b) R. Capelli, S. Toffanin, G. Generali, H. Usta, A. Facchetti, M. Muccini, *Nat. Mater.* **2010**, *9*, 496; c) H. Usta, W. C. Sheets, M. Denti, G. Generali, R. Capelli, S. Lu, X. Yu, M. Muccini, A. Facchetti, *Chem. Mater.* **2014**, *26*, 6542; d) S. Hotta, T. Yamao, S. Z. Bisri, T. Takenobu, Y. Iwasa, *J. Mater. Chem. C* **2014**, *2*, 965.
- [2] a) G. Schwartz, M. Pfeiffer, S. Reineke, K. Walzer, K. Leo, *Adv. Mater.* **2007**, *19*, 3672; b) T. Zheng, W. C. H. Choy, *Adv. Funct. Mater.* **2010**, *20*, 648; c) Y.-L. Lei, Y. Jin, D.-Y. Zhou, W. Gu, X.-B. Shi, L.-S. Liao, S.-T. Lee, *Adv. Mater.* **2012**, *24*, 5345; d) T. O. McDonald, P. Martin, J. P. Patterson, D. Smith, M. Giardiello, M. Marcello, V. See, R. K. O'Reilly, A. Owen, S. Rannard, *Adv. Funct. Mater.* **2012**, *22*, 2469.
- [3] a) S. Z. Bisri, T. Takenobu, Y. Yomogida, H. Shimotani, T. Yamao, S. Hotta, Y. Iwasa, *Adv. Funct. Mater.* **2009**, *19*, 1728; b) T. Yamao, Y. Sakurai, K. Terasaki, Y. Shimizu, H. Jinnai, S. Hotta, *Adv. Mater.* **2010**, *22*, 3708; c) S. Z. Bisri, T. Takenobu, K. Sawabe, S. Tsuda, Y. Yomogida, T. Yamao, S. Hotta, C. Adachi, Y. Iwasa, *Adv. Mater.* **2011**, *23*, 2753; d) S. Z. Bisri, K. Sawabe, M. Imakawa, K. Maruyama, T. Yamao, S. Hotta, Y. Iwasa, T. Takenobu, *Sci. Rep.* **2012**, *2*, 985; e) H.-H. Fang, R. Ding, S.-Y. Lu, J. Yang, X.-L. Zhang, R. Yang, J. Feng, Q.-D. Chen, J.-F. Song, H.-B. Sun, *Adv. Funct. Mater.* **2012**, *22*, 33; f) H. Shang, H. Shimotani, S. Ikeda, T. Kanagasekaran, K. Oniwa, T. Jin, N. Asao, Y. Yamamoto, H. Tamura, K. Abe, M. Kanno, M. Yoshizawa, K. Tanigaki, *J. Phys. Chem. C* **2017**, *121*, 2364; g) J. Gierschner, S. Y. Park, *J. Mater. Chem. C* **2013**, *1*, 5818; h) S. K. Park, J. H. Kim, T. Ohto, R. Yamada, A. O. F. Jones, D. R. Whang, I. Cho, S. Oh, S. H. Hong, J. E. Kwon, J. H. Kim, Y. Olivier, R. Fischer, R. Resel, J. Gierschner, H. Tada, S. Y. Park, *Adv. Mater.* **2017**, *29*, 7.
- [4] a) H. Wang, F. Li, B. Gao, Z. Xie, S. Liu, C. Wang, D. Hu, F. Shen, Y. Xu, H. Shang, Q. Chen, Y. Ma, H. Sun, *Cryst. Growth Des.* **2009**, *9*, 4945; b) H. Nakanotani, C. Adachi, *Adv. Opt. Mater.* **2013**, *1*, 422; c) R. Ding, J. Feng, F. X. Dong, W. Zhou, Y. Liu, X. L. Zhang, X. P. Wang, H. H. Fang, B. Xu, X. B. Li, H. Y. Wang, S. Hotta, H. B. Sun, *Adv. Funct. Mater.* **2017**, *27*, 1604659.
- [5] J. R. Lakowicz, in *Principles of Fluorescence Spectroscopy* (Ed: J. R. Lakowicz), Springer, Boston, MA, USA **2006**.
- [6] H.-H. Fang, S.-Y. Lu, L. Wang, R. Ding, H.-Y. Wang, J. Feng, Q.-D. Chen, H.-B. Sun, *Org. Electron.* **2013**, *14*, 389.
- [7] H. H. Lu, C. Y. Liu, C. H. Chang, S. A. Chen, *Adv. Mater.* **2007**, *19*, 2574.
- [8] B. Russ, M. J. Robb, F. G. Brunetti, P. L. Miller, E. E. Perry, S. N. Patel, V. Ho, W. B. Chang, J. J. Urban, M. L. Chabiny, C. J. Hawker, R. A. Segalman, *Adv. Mater.* **2014**, *26*, 3473.
- [9] a) V. A. Postnikov, Y. I. Odarchenko, A. V. Iovlev, V. V. Bruevich, A. Y. Pereverzev, L. G. Kudryashova, V. V. Sobornov, L. Vidal, D. Chernyshov, Y. N. Luponosov, O. V. Borshchev, N. M. Surin, S. A. Ponomarenko, D. A. Ivanov, D. Y. Paraschuk, *Cryst. Growth Des.* **2014**, *14*, 1726; b) L. G. Kudryashova, M. S. Kazantsev, V. A. Postnikov, V. V. Bruevich, Y. N. Luponosov, N. M. Surin, O. V. Borshchev, S. A. Ponomarenko, M. S. Pshenichnikov, D. Y. Paraschuk, *ACS Appl. Mater. Interfaces* **2016**, *8*, 10088; c) Y. Inada, T. Yamao, M. Inada, T. Itami, S. Hotta, *Synth. Met.* **2011**, *161*, 1869.
- [10] R. Katoh, K. Suzuki, A. Furube, M. Kotani, K. Tokumaru, *J. Phys. Chem. C* **2009**, *113*, 2961.
- [11] C. A. Parker, *Photoluminescence of Solutions*, Elsevier, NY, USA **1968**.
- [12] a) T.-S. Ahn, R. O. Al-Kaysi, A. M. Müller, K. M. Wentz, C. J. Bardeen, *Rev. Sci. Instrum.* **2007**, *78*, 086105; b) M. S. Kazantsev, E. S. Frantseva, L. G. Kudryashova, V. G. Konstantinov, A. A. Mannanov, T. V. Rybalova, E. V. Karpova, I. K. Shundrina, G. N. Kamaev, M. S. Pshenichnikov, E. A. Mostovich, D. Y. Paraschuk, *RSC Adv.* **2016**, *6*, 92325.
- [13] A. Köhler, H. Bässler, *Electronic Processes in Organic Semiconductors: An Introduction*, Wiley-VCH Verlag GmbH & Co. KGaA, Weinheim, Germany **2015**, ch. 1.
- [14] a) V. Podzorov, *MRS Bull.* **2013**, *38*, 15; b) G. Horowitz, *J. Mater. Res.* **2011**, *19*, 1946.
- [15] V. P. Ananikov, L. L. Khemchyan, V. I. Yu, V. I. Bukhtiyarov, A. M. Sorokin, I. P. Prosvirin, S. Z. Vatsadze, A. V. Medved'ko, V. N. Nuriev, A. D. Dilman, V. V. Levin, I. V. Koptuyug, K. V. Kovtunov, V. V. Zhivonitko, V. A. Likhobolov, A. V. Romanenko, P. A. Simonov, V. G. Nenajdenko, O. I. Shmatova, V. M. Muzalevskiy, M. S. Nechaev, A. F. Asachenko, O. S. Morozov, P. B. Dzhevakov, S. N. Osipov, D. V. Vorobyeva, M. A. Topchiy, M. A. Zotova, S. A. Ponomarenko, O. V. Borshchev, N. L. Yu, A. A. Rempel, A. A. Valeeva, A. Y. Stakheev, O. V. Turova, I. S. Mashkovsky, S. V. Sysolyatin, V. V. Malykhin, G. A. Bukhtiyarova, A. O. Terent'ev, I. B. Krylov, *Russ. Chem. Rev.* **2014**, *83*, 885.
- [16] C. B. Aakeroy, D. J. Salmon, *CrystEngComm* **2005**, *7*, 439.
- [17] H. J. Egelhaaf, J. Gierschner, D. Oelkrug, *Synth. Met.* **2002**, *127*, 221.
- [18] a) A. Serbenta, O. V. Kozlov, G. Portale, P. H. M. van Loosdrecht, M. S. Pshenichnikov, *Sci. Rep.* **2016**, *6*, 36236; b) O. V. Kozlov, F. de Haan, R. A. Kerner, B. P. Rand, D. Cheyns, M. S. Pshenichnikov, *Phys. Rev. Lett.* **2016**, *116*, 57402.
- [19] T. Y. Starikova, N. M. Surin, O. V. Borshchev, S. A. Pisarev, E. A. Svidchenko, Y. V. Fedorov, S. A. Ponomarenko, *J. Mater. Chem. C* **2016**, *4*, 4699.
- [20] Y. A. Getmanenko, R. J. Twieg, *J. Org. Chem.* **2008**, *73*, 830.
- [21] V. Podzorov, S. E. Sysoev, E. Loginova, V. M. Pudalov, M. E. Gershenson, *Appl. Phys. Lett.* **2003**, *83*, 3504.